Star Formation Triggering Mechanisms in Dwarf Galaxies: The Far-Ultraviolet, Hα, and HI Morphology of Holmberg II

Susan G. Stewart[1]
U. S. Naval Observatory, 3450 Massachusetts Ave NW, Washington, DC 20392-5420

Michael N. Fanelli
Dept. of Physics, University of North Texas, Denton, TX 76203

Gene G. Byrd
Dept. of Physics and Astronomy, University of Alabama, Tuscaloosa, AL 35487

Jesse K. Hill
Hughes STX, 4400 Forbes Blvd., Lanham, MD 20706

David J. Westpfahl
Dept. of Physics, New Mexico Institute of Mining & Technology, Socorro, NM 87801

Kwang-Ping Cheng
Dept. of Physics, California State University, Fullerton, CA 92634

Robert W. O'Connell
University of Virginia, P.O. Box 3818, Charlottesville, VA 22903

Morton S. Roberts
National Radio Astronomy Observatory, Edgemont Rd., Charlottesville, VA 22903

Susan G. Neff, Andrew M. Smith, and Theodore P. Stecher
Laboratory for Astronomy and Solar Physics, NASA/GSFC, Greenbelt, MD 20771

ABSTRACT

Far-ultraviolet (FUV), Hα, and HI observations of dwarf galaxy Holmberg II are used to investigate the means by which star formation propagates in galaxies lacking

[1]NASA Space Grant Fellow, University of Alabama 1995-1997

global internal triggering mechanisms such as spiral density waves. The observations trace the interaction between sites of massive star formation and the neutral and ionized components of the surrounding ISM in this intrinsically simple system. Both local and large-scale triggering mechanisms related to massive star formation are seen, suggesting that feedback from massive stars is a microscopic process operating in all galaxies to a certain degree.

The data emphasize the importance of local conditions in regulating star formation from evidence such as massive stars inside ionized shells, compact HII regions surrounding aging clusters, and stars formed in chains of progressing age. Surface brightness profiles show current activity correlates with the time averaged level of past star formation at a given radius demonstrating a reliance on local conditions. Large-scale triggering by HI shells is supported by observations of progenitor populations as well as secondary sites of star formation associated with their dense rims. Analysis of the energy available from massive stars inside HI shells indicates energy deposited into the ISM from supernovae and stellar winds is sufficient to account for the HI morphology. Ages of individual star forming regions are derived using B, Hα, and FUV photometry and show both older, diffuse FUV regions and younger, compact HII regions. The distribution of ages is reconciled with the HI morphology, showing a clear preference of young regions for areas of dense HI and old regions for HI voids. Global kinematical properties may also play a role in the star formation process since differences in the rotation characteristics of the neutral gas disk correlate with differences in triggering mechanisms. Large-scale feedback from massive stars is shown to operate in regions that lack differential shear in the gas disk.

Subject headings: galaxies: individual (DDO 50) – ISM: HII regions, bubbles – stars: formation – ultraviolet: general

1. Introduction

The pervading questions surrounding our current view of large-scale star formation are primarily associated with the need to understand the mechanism for triggering and globally maintaining star formation. The first step in forming a fundamental theory to describe star formation in all environments is understanding the process in intrinsically simple systems. This study utilizes a unique observational dataset to explore the processes which may influence new star formation and its relation to the ISM within a relatively uncomplicated dynamical environment. Far-ultraviolet (FUV), Hα, and HI images of dwarf galaxy Holmberg II (HoII) are used to gain new insight into the star formation process by studying the interconnection between massive star formation and the ionized and neutral components of the galaxy's ISM.

Irregular galaxies lack a dominant internal global triggering mechanism for cloud compression and star formation such as density waves, yet exhibit a wide range of star formation activity. Non-interacting low surface brightness late-type galaxies, including Magellanic-type irregulars (Im), are ideal for this study due to the limited number of global internal processes influencing star formation while at the same time having star formation rates per unit area similar to much more massive spiral galaxies (Hunter 1997). Due to their small size, the amount of energy input per a given star formation event has a pronounced effect on the global ISM. Instabilities in the ISM introduced by massive star formation may play an important role in the star formation process in these systems. They display relatively uncomplicated internal gas dynamics, generally characterized as slow solid body rotation. These characteristics create an environment of reduced shear allowing features in the ISM to be longer lived. They often possess huge gas envelopes extending well beyond the optical regime of the galaxy. Large vertical scale heights allow features in the ISM to grow to large sizes before breaking out of the HI layer. In addition, these systems allow for the test of star formation models at very low metallicities. For these reasons, late-type low surface brightness galaxies are powerful tools for understanding the star formation process and galaxy evolution.

The apparently non-interacting Im-type galaxy HoII (DDO 50, UGC 4305) is a member of the M81-NGC 2403 group of galaxies. The galaxy is classified as a David Dunlap Observatory (DDO) dwarf galaxy due to its low surface brightness (van den Bergh 1959). Although it is slightly too bright to fit the magnitude criterion of a "true dwarf" galaxy of $M_B \gtrsim -16$ (Nilson 1973), it is usually referred to as a dwarf galaxy in the literature. IRAS observations of HoII suggest a minimal presence of dust, so little hidden star formation is taking place (Hunter *et al.* 1989). The galaxy has a low metal abundance, $Z/Z_\odot \sim 0.4$ (Hunter & Gallagher 1985), similar to that of the Large Magellanic Cloud (LMC). Hodge *et al.* (1994) find that the sizes of HII regions as well as their size distribution are statistically normal in comparison to galaxies of the same type, distance, and luminosity. HoII has a HI envelope extending to 1.5 D_{Ho}, where the Holmberg diameter (D_{Ho}) is the diameter defined by the B isophote at 26.6 mag arcsec^{-2}. The HI morphology of HoII is intriguing due to the various shells and holes present throughout the galaxy (Puche *et al.* 1992). Hoessel *et al.* (1998) estimate a distance of 3.05 Mpc using 28 Cepheid candidates. This is different than the distance estimate of 3.63 Mpc determined by Freedman *et al.* (1994) for M81 using Hubble Space Telescope observations of Cepheid variables. Since HoII is likely the closest member of the M81-NGC 2403 group, 3.05 Mpc is adopted for the distance of HoII. Table 1 summarizes the parameters assumed for the galaxy in this study.

Observations in the vacuum ultraviolet (UV, $\lambda\lambda$ 912 - 3200 Å) isolate hot sources from the underlying optical cool star background in galaxies. Ultraviolet observations allow direct detection of young massive stars, which are responsible for the majority of photoionization, photodisassociation, elemental synthesis, and kinetic energy input in galaxies. The UV observations used in this study are in the FUV window ($\lambda\lambda$912 - 2000 Å) and are particularly useful in characterizing high-mass star formation since the dominant luminosity sources at 1500 Å are OB stars with mass $M \gtrsim 5\ M_\odot$(Fanelli *et al.* 1992). Understanding the UV morphology and its relation to the star formation process has broad implications considering that the rest frame FUV is detectable at high redshift, $z \gtrsim 3$, with optical and IR instruments. O'Connell (1997) stresses that determining a "morphological k-correction" for galaxies is needed to assess the morphology of distant objects. Therefore, understanding the processes responsible for the UV emission in nearby systems will play an important role in advancing our understanding of galaxy evolution.

Parameter		Value	Reference
Optical Center	α_{1950}	$8^h\ 13^m\ 53\overset{s}{.}5$	Dressel & Condon (1976)
	δ_{1950}	$70°52'13''$	
Dynamical Center	α_{1950}	$8^h\ 13^m\ 53^s$	Westpfahl (1997)
	δ_{1950}	$70°52'47\overset{''}{.}3$	
Distance		3.05 Mpc	Hoessel, Saha, & Danielson (1998)
M_B		-16.52	RC3, de Vaucouleurs *et al.* (1991)
Inclination		$41°$	Puche *et al.* (1992)
Position Angle		$177°$	Puche *et al.* (1992)
Axial Ratio, q=b/a		0.74	Huchtmeier & Richter (1988)
A_B		0.10	RC3, de Vaucouleurs *et al.* (1991)
A_{FUV}		0.20	This study

Table 1: Adopted Parameters for Holmberg II

This study addresses several issues which Hunter (1997) stresses are vital to an improved understanding of star formation processes within irregular galaxies. These key issues are tied to the need for a better understanding of the regulation mechanism for star formation on global and local scales, including a quantitative description of both the feedback processes operating in irregular galaxies and the impact which huge stellar complexes have on the surrounding ISM. Morphological comparisons between the FUV flux and other radiation linked to star formation provide valuable information regarding the interaction between a star forming site and its surrounding medium. For example, the ratio of the FUV and Hα emission from a young star forming region is indicative of the cluster age. The suggested link between massive star formation and HI shells can be studied via the relative FUV and HI emission morphologies. Since the FUV is able to isolate the massive stellar component over timescales similar to the kinematic ages of HI shells, this comparison could identify a progenitor population. Understanding if characteristic differences in the ISM are related to differences in star formation mechanisms is another important issue. The FUV image can be used to probe the possible relationship between massive star formation and the kinematics of its HI disk. The intrinsic dynamical reduction of shear in the gas disks compared to spiral galaxies most likely influences the overall star formation rate.

Despite the wealth of information provided by UV images, they are seldomly used in star formation studies because spatially-resolved UV images are rare. The FUV images used in this study are provided by the Ultraviolet Imaging Telescope (UIT) which flew as a member of the ASTRO Observatory on two Shuttle missions in December, 1990 and March, 1995. Together, a total of $\sim$ 35 FUV images of galaxies exhibiting recent star formation were observed. The $\sim 3''$ spatial resolution of the UIT was a 5$-$20 times improvement over previously available UV imagery. Besides the Apollo 16 UV image of the LMC in 1972 (Page & Carruthers 1981), the only other UV image of a galaxy similar in type to HoII prior to the ASTRO-2 mission was the dwarf galaxy Holmberg IX. It was serendipitously observed during the ASTRO-1 mission due to its close proximity to M81. Using the UV data, Hill *et al.* (1993) characterized the most recent star formation event, confirming that no recent star formation was occurring in Holmberg IX. During the second flight of the UIT, a dwarf galaxy program was initiated. The results of this program were first presented by Gessner *et al.* (1995). Detailed analysis of all of the UIT dwarf galaxy targets is presented by Stewart (1998).

Global photometry of the galaxy is given in §3 and the radial surface brightness profiles in §4. Photometry of individual star forming complexes along with their derived ages and internal extinctions are presented in §5. Comparisons between the relative morphologies of the FUV and Hα emission are given in §6 and that of the FUV and HI in §7. The principal results are summarized in §8.

2. Observations and Data Reduction

Holmberg II was observed by the UIT during the ASTRO-2 mission in March, 1995. Table 2 summerizes the observations of the galaxy used in this study. The targets were observed using the broad-band UIT B1 filter, which has $\lambda_{eff} = 1521$ Å and $\Delta\lambda = 354$ Å. The images were recorded on IIaO film and digitized with a PDS microdensitometer at Goddard Space Flight Center, producing 2048×2048 pixel images with scale $1\farcs14$ pixel^{-1}. The images were calibrated using IUE spectrophotometry of stars observed by the UIT. The FUV magnitudes are computed from FUV flux using $m_{FUV} = -2.5\times \log_{10}(\mathrm{FUV}) - 21.1$, where FUV is the incident flux in erg (cm^{2}Å s)$^{-1}$. The chief photometric uncertainties are in the form of low-level nonuniformities introduced via the development and digitization processes. Uncertainty in the absolute calibration can lead to uncertainties of up to 10 − 15 % in the FUV flux. A detailed discussion of the reduction of the UIT data to flux-calibrated arrays is given by Stecher *et al.* (1992, 1997).

The FUV background level ($\mu > 25$ mag arcsec^{-2}) is checked by taking the mean of 20, 20×20 pixel boxes in areas void of any galaxy or stellar flux. The FUV background level is minimal, 0.0±0.4 analog data units (ADU's). The UIT has limited accuracy at the lowest light levels. The error in the background level reflects this intrinsic uncertainty.

CCD observations of HoII were obtained in the Johnson U and B bands, and the Kron-Cousins R and Hα bands with San Diego State University's 1.0 m telescope at the Mount Laguna Observatory (MLO). The optical images are median combined with at least two other images having the same exposure time to remove cosmic rays and other defects. Astrometry and photometry are implemented using standard IDL procedures for data reduction. Background values are determined for each image by taking the mean of pixels in 20, 10×10 pixel boxes. The HoII broad-band images are calibrated using unpublished photoelectric photometry of three bright stars in the galaxy (Corwin 1997). Total magnitudes given in the RC3 agree with our measured values within reasonable limits providing a check of the calibration constants.

The Hα filter at MLO has a centroid wavelength 6573 Å and width 61 Å which includes the [N II] lines. A correction for this contribution to the Hα flux is made by assuming f (Hα) / (f (Hα) + f ([N II])) ≈ 0.88, based on spectral observations of H II regions by Hunter & Gallagher (1985). This correction is applied using the calibration technique of Waller (1990) and observations of the Hα standard star BD +8°2015 (Stone 1977). Attempting to reproduce the irregular apertures defined by Hodge *et al.* (1994) for H II regions in HoII provides a check for the Hα calibration constant. Our photometry of these regions agree within ∼ 9 %. Deviations may be caused by failure to reproduce the irregular apertures exactly. An Hα emission image is produced by scaling stars in the Hα image with those in the R-band image and subtracting the stellar continuum component.

The 21 cm images were obtained with the VLA B, C, and D arrays. The uniformly weighted column density map has a spatial resolution of $4'' \times 4\farcs5$, corresponding to a spatial resolution of 60 pc at the distance of HoII. This image is used in the Puche *et al.* (1992) study of HoII where a complete description of its observational characteristics is given.

3. Global Photometry

In Figure 1a the $10\farcm0 \times 10\farcm0$ FUV image of HoII is presented. The FUV morphology is quite patchy with the brightest features contained in a central star forming arc. There is a region of diffuse FUV emission extending to the southwest and three separate patches of FUV emission to the north of the central arc.

Since galaxies at high redshift are seen in the rest frame FUV with optical instruments, the FUV image is compared to the R-band image in Figure 1b to illustrate the importance of understanding the FUV morphology of local galaxies. The R-band image of the galaxy exhibits a relatively smooth distribution of light compared to the irregular distribution shown by the FUV image. The true optical morphology of a high redshift galaxy could be quite different than that observed in the optical bands.

Integrated magnitudes of HoII are obtained using elliptical apertures whose shape and orientation are based upon the derived HI structural parameters given in Table 1. The dynamical center is adopted as the aperture center since it has more physical significance than the optical center, especially when comparing integrated parameters from observations ranging from the R-band to the FUV. The optical magnitudes are derived using images with the foreground stars masked, the brightest of which are given the average flux from the surrounding medium. Therefore, the derived magnitudes may be slightly less than pub-

Telescope	Filter	Exposure Time (s)	Date
UIT	FUV (B1)	1310	Mar 11, 1995
MLO	U	1200	Nov 2, 1995
MLO	B	300	Feb 24, 1995
MLO	R	120	Feb 24, 1995
MLO	Hα	600	Feb 24, 1995

Table 2: Summary of Observations for Holmberg II

lished catalog values. Since the FUV image is free from foreground star contamination, foreground stars are masked from optical images in order to make a true comparison with the FUV band. The total integrated magnitudes, corrected for Galactic extinction, A_g, are given for each bandpass in Table 3. Galactic extinction in the FUV is derived assuming the Galactic reddening curve of Savage and Mathis (1979) integrated over the UIT B1 bandpass. These are related by A_{FUV} / E(B−V) = 8.33 (Hill *et al.* 1997). The errors account for the photometric uncertainty and ∼7% uncertainty in the distance estimate. Corrections for internal extinction will be discussed later (§5.2).

The FUV magnitude is at the faint end of the range of absolute magnitudes observed by the UIT. In a sample of 35 galaxies exhibiting recent massive star formation, the range of observed absolute magnitudes spans from −17 to −22 (Fanelli *et al.* 1997b). The corresponding FUV−B = −1.74±0.03 color falls into the range observed by FAUST (a balloon-born UV camera) for a sample of Im-type galaxies (Deharveng *et al.* 1994).

The integrated FUV flux as a function of radius provides information regarding the concentration of recent massive star formation. The FUV growth curve, corrected for Galactic extinction, is shown in Figure 2. It illustrates that recent massive star formation is not particularly centrally concentrated in HoII despite the presence of the prominent central star forming arc. The aperture containing this feature in its entirety (1.′7) only contains ∼43% of the total FUV flux. Therefore, massive star formation extends well beyond the central star forming arc.

3.1. Global Star Formation Rates

The intrinsic emission of a young stellar population can be translated into a global star formation rate (SFR) by comparing integrated fluxes with predictions from stellar population synthesis models. The timescale characterized by a given SFR depends upon the bandpass of the observation since the luminosity of a single generation of stars decays roughly as a power law (O'Connell 1997). The Lyman continuum (Balmer emission lines) describes the SFR over a timescale $\lesssim$ 5 Myr while the UV continuum characterizes the SFR over a 100 Myr timescale. Since massive stars ($M \gtrsim 10 M_\odot$) are the ionizing sources for the Lyman continuum, observed here via the Hα recombination line, and the UV emission is dominated by stars $\gtrsim 5 M_\odot$, the SFR derived using these bandpasses describes the formation history of massive stars. Late-type irregular galaxies are dominated by short-lived massive stars and are therefore excellent sources to provide an estimate of the SFR using either FUV or Hα observations.

The global SFR for massive stars in HoII is derived using both the integrated FUV and Hα flux by applying formulae which convert the integrated light from each bandpass to an estimate of the global SFR. These formulae are taken from Kennicutt (1998) who provides a self-consistent set of formulae for various regimes based on the calibration of Madau *et al.* (1998) for a fixed Salpeter (1955) IMF with mass limits 0.1 to 100 $M_\odot$. The observed (not corrected for internal extinction) FUV and Hα luminosity and global SFR are listed in Table 4. The Hα luminosity and $SFR_{H\alpha}$ agree reasonably well with the values derived by Miller & Hodge (1994) after differences in distances are removed.

Since internal extinction is not extreme low metallicity systems, the comparison between $SFR_{H\alpha}$ and

Filter	Apparent Magnitude	Absolute Magnitude	A_g
FUV	9.84±0.03	-17.58 ± 0.15	0.20
U	11.48±0.02	-15.94 ± 0.15	0.12
B	11.58±0.02	-15.84 ± 0.15	0.10
R	10.86±0.01	-16.56 ± 0.15	0.06

Table 3: Integrated Magnitudes for Holmberg II

NOTE.—Magnitudes are corrected for Galactic extinction. Optical magnitudes are derived with the foreground stars masked.

$\mathrm{Log(L_{H\alpha})}$	$\mathrm{Log(L_{FUV})}$	$\mathrm{SFR_{H\alpha}}$ $\mathrm{M_\odot yr^{-1}}$	$\mathrm{SFR_{FUV}}$ $\mathrm{M_\odot yr^{-1}}$	$\mathrm{SFR_{FUV}/SFR_{H\alpha}}$
39.55	38.67	0.028	0.049	1.75

Table 4: Global Star Formation Rates for Holmberg II

NOTE.—Rates are not corrected for extinction internal to HoII.

$\mathrm{SFR_{FUV}}$ is valid to the first order in estimating the recent to current formation history of massive stars. For example, differences in internal extinction effects between the FUV and Hα observations for a given E(B-V) are likely on the order of $\mathrm{A_{FUV}/A_{H\alpha}} \sim 4$, assuming a LMC extinction curve for internal reddening (this ratio doubles for the SMC extinction curve). This difference translates into a higher $\mathrm{SFR_{FUV}}$ than $\mathrm{SFR_{H\alpha}}$ in a given system by underestimating $\mathrm{A_{FUV}}$ to a greater degree than $\mathrm{A_{H\alpha}}$. The results indicate the "recent" (traced by the FUV) and "current" (traced by Hα) massive star formation rates are comparable. The ratio $\mathrm{SFR_{FUV}}$ to $\mathrm{SFR_{H\alpha}}$ indicates that the FUV flux traces a slightly larger fraction of massive star formation than the Hα flux, perhaps suggesting HoII is in a post-burst phase.

4. Radial Dependence of Star Formation

Surface brightness profiles are derived using magnitudes corrected for Galactic foreground extinction in elliptical annuli 16″ wide. The optical profiles are created using images with the foreground star component masked; the brightest of these stars is given the average value from their surroundings. To effectively compare the behavior of surface brightness profiles of irregular-type galaxies, the choice of aperture center is important. As with the integrated magnitudes, the dynamical center is chosen as the aperture center instead of the optical center or brightest feature in order to make a uniform physical comparison with other galaxies.

4.1. FUV Surface Brightness Profiles

The patchy distribution of FUV light shown in the UIT image is represented in the surface brightness profiles by pronounced inflections at various radii. The FUV surface brightness profile, shown in Figure 3, has a double peaked shape with a central depression. At the aperture center, the average surface brightness is μ_{FUV}=21.6 mag arcsec^{-2}±0.11 while at the first peak, 0.′9 from the center, the average value is μ_{FUV}=21.2 mag arcsec^{-2} ± 0.03. Surface brightness maps of the galaxy indicate that the highest levels of activity lie in the region responsible for this peak; the brightest knot in the center of the star forming arc has the highest levels, μ_{FUV} ∼18.9 mag arcsec^{-2} in a resolution element (5″). Following the peak, the profile exhibits somewhat exponential behavior until r∼2′, where it takes a constant value of μ_{FUV} ∼22.4 mag arcsec^{-2}. The flattening of the profile is due to flux from the group of regions on the eastern side of the central star forming arc. A second, yet relatively

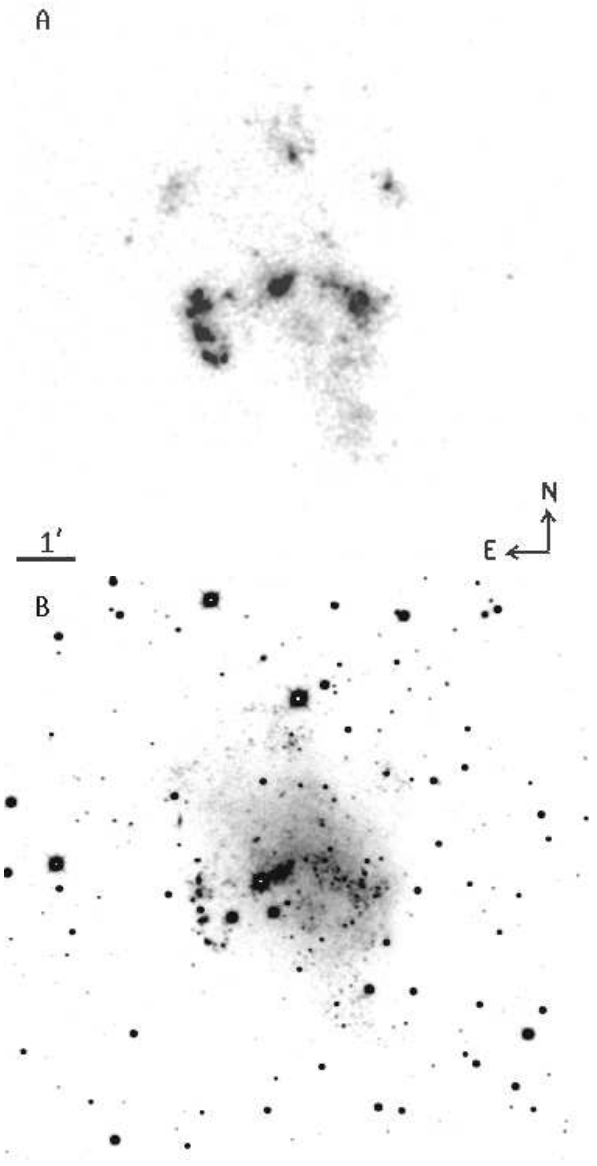

Fig. 1.— Registered FUV (A, top) and R-band images (B, bottom) of Holmberg II.

small peak occurs at r∼2.7′, after which it falls off sharply. The second peak can be accounted for by the diffuse patches of emission in the northern part of the galaxy.

The sample of FUV surface brightness profiles presented by Stewart (1998) offers little uniformity with regard to identifying characteristics for late-type low surface brightness systems. It is a relatively heterogeneous group which does not follow either a characteristic $R^{1/4}$ law or a pure exponential. However, some general trends do emerge which could have important implications in interpreting optical observations of high redshift galaxies where the observed light is the redshifted UV continuum. These characteristics are also exhibited by the HoII profile: generally flat with inflections associated with prominent star forming complexes, healthy activity far from the galaxy center, and non-centralized organization of star formation. As compared to FUV profiles of other galaxies observed by the UIT, the HoII profile has characteristics somewhat similar to those of IBm-type galaxy NGC 4449 (Fanelli *et al.* 1997a). NGC 4449 has an exponential FUV surface brightness profile with inflections due to blue knots (Hill *et al.* 1998). The profile does not have a central light depression, but this may be due to the choice of the aperture center. Although steeper than the HoII profile, the NGC 4449 profile shows similar characteristic inflections due to star formation at large radii from the center.

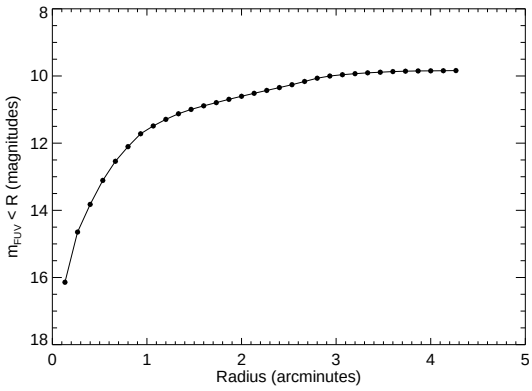

Fig. 2.— The FUV growth curve of Holmberg II.

4.2. Optical Surface Brightness Profiles

In contrast to the lack of FUV profiles, there have been numerous studies characterizing the optical light profiles of low surface brightness galaxies (Karachentseva *et al.* 1996; Patterson & Thuan 1996; Vader & Chaboyer 1994). The B-band profile of HoII, shown in Figure 4, can be characterized as exponential with a central depression. This behavior is typical of late-type low surface brightness galaxies. The underlying exponential component indicates the presence of an optical disk superimposed on bright star forming knots while the central trough demonstrates that star formation is not centrally organized around a nucleus.

A rough estimate of the central surface brightness of the HoII B-band profile is made by fitting it with a pure exponential which is extrapolated to the center of the galaxy. Corrected for Galactic foreground extinction, $\mu_{\rm B}(0)$=22.3±0.02 mag arcsec^{-2}. The range in central surface brightness of the galaxies in the Karachentseva *et al.* (1996) sample is 22.2 $\lesssim \mu_{\rm B}(0) \lesssim$ 24 mag arcsec^{-2} compared to the canonical value of 21.65 ±0.30 mag arcsec^{-2} for disk galaxies (Freeman 1970). Holmberg II falls at the brighter end of the observed range for low surface brightness irregular galaxies. Other studies report an average $\langle\mu_{\rm B}(0)\rangle$=23.5±0.2 (Rönnback and Bergvall 1994) and $\langle\mu_{\rm B}(0)\rangle$=23.5±1.6 mag arcsec^{-2} (Vader & Chaboyer 1994).

4.3. Radial Continuity of Star Formation

The general lack of correlation between star formation properties and other global properties such as abundance or global gas parameters in irregular galaxies suggests that local rather than global conditions are important in regulating star formation. For example, Hunter, Elmegreen, & Baker (1998) do not find a correlation between the star formation and the ratio of the HI surface density to the critical density for gas instabilities in a sample of dwarf irregular galaxies, while the stellar surface brightness does correlate with this ratio. These results suggest that stellar energy provides feedback for star formation to a certain degree. Studies of the radial dependence of the optical and Hα emission also suggest that local regulation of star formation may be important in both irregular (Hunter & Gallagher 1985) and spiral galaxies (Ryder & Dopita 1994). The FUV bandpass gives some insight into the radial dependence of the recent star formation activity, yet over longer

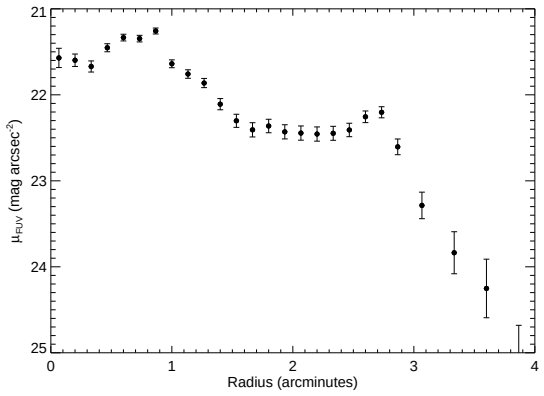

Fig. 3.— The FUV surface brightness profile of Holmberg II.

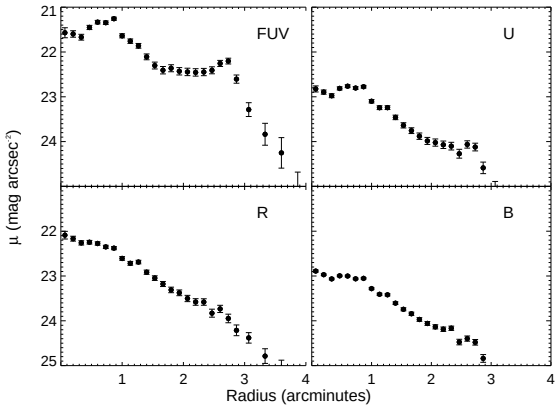

Fig. 4.— Optical and FUV surface brightness profiles of Holmberg II.

timescales than the Hα emission allows. Figure 4 displays the FUV, U, B, and R-band profiles of HoII on the same linear scale. Beginning with the R-band profile and moving counterclockwise around the figure, the profiles become less smooth as the wavelength of the profile decreases. This is expected due to the contribution from recent star formation, while at increasingly longer wavelengths, the light is more complicated measure of the entire history of star formation. The general shape of each profile is same and the radii at which increased star formation activity occurs remains relatively constant over the timescale which these profiles track star formation activity, roughly a few Gyrs. Figure 4 suggests that HoII is currently forming stars at the same radii as it has in the past, supporting the supposition that star formation in irregular galaxies is a local process and that local conditions such as gas distributions and feedback from massive stars may play a significant role in the star formation process.

5. Properties of Star Forming Regions

Star forming properties are examined in further detail by characterizing the individual star forming complexes. Star formation for individual regions is quantified by means of photometry in the observed bandpassses, used to derive a characteristic age and internal extinction for each region. The physical property upon which the age derivation is based is the different timescale of decay of the Hα and FUV flux from an evolving cluster. The Hα emission from an evolving cluster peaks at roughly 1-2 Myr and falls off sharply. The FUV emission coming directly from the young massive stars in an evolving cluster peaks at roughly 5 Myr and decays on a much longer timescale than the Hα emission (see O'Connell 1997, Fig. 1).

5.1. Photometry of Star Forming Regions

Star formation regions are defined by selecting regions of associated FUV and Hα flux. Since both the FUV and Hα emission define a star forming region in this context, the ages provide a snapshot of the pattern of star formation over a 100 Myr timescale. This is an unconventional approach in defining the spatial distribution of young star formation which is normally described by Hα observations alone. The registered FUV and continuum subtracted Hα images of HoII are compared in Figure 5 to highlight the differences between the spatial patterns of current and recent star

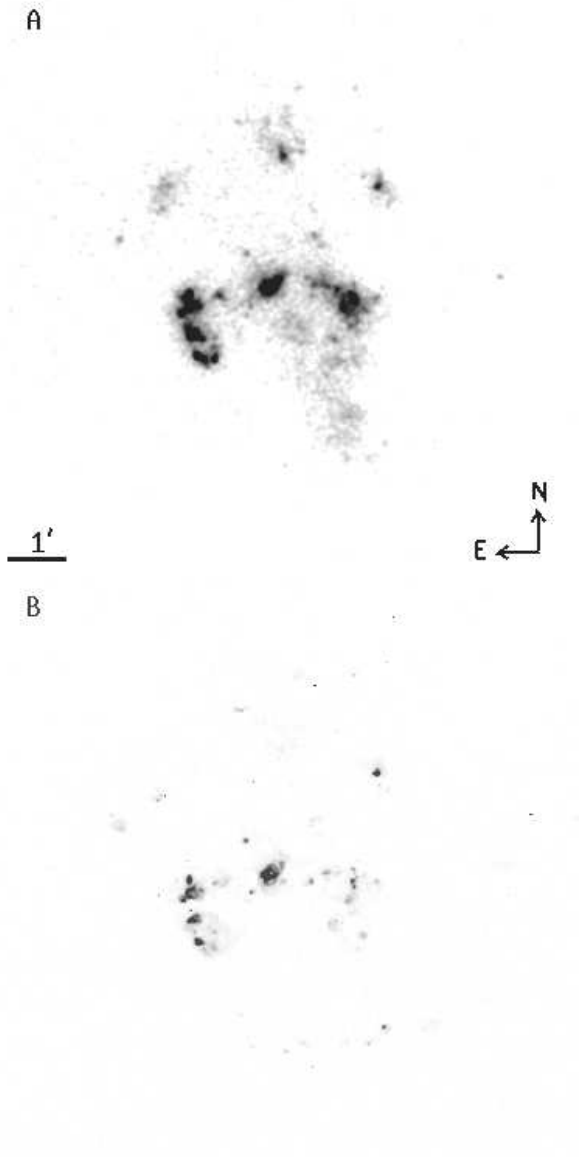

Fig. 5.— Registered FUV (A, top) and Hα (B, bottom) images of Holmberg II.

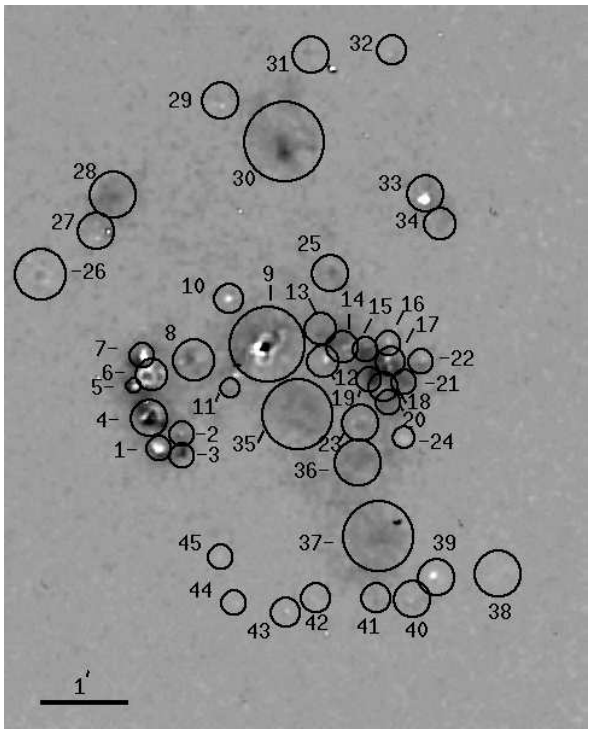

Fig. 6.— Holmberg II star formation regions on a FUV, Hα difference image; areas with Hα and no FUV emission are white and areas with FUV and no Hα emission are black.

formation activity.

The choice of region boundary is facilitated by creating a FUV and Hα difference image, which reveals areas of associated emission. Circular apertures are drawn so as to include HII regions defined in previous studies (Hodge *et al.* 1994) and approximately all FUV emission above a limiting surface brightness of 21.5 mag arcsec^{-2}. Using these criteria, 45 regions are identified. The apertures are drawn on a FUV, Hα difference image in Figure 6. Some regions are defined by virtue of meeting this criteria in only one of the two bandpasses. The choice of aperture size is straightforward when associated emission is compact and coincident. Ideally, an aperture would contain only a coeval association and its immediate HII regions. However, the resolution of the image limits the ability to select a single generation of star formation. The effect which sampling slightly different ages in a single aperture has on the subsequent derivations is discussed below.

The FUV, B, and continuum subtracted Hα flux are measured for each region. A correction for the background light internal to the galaxy is made for the B-band photometry by averaging the values immediately surrounding a region. Since this quantity may be variable for some regions, especially the larger ones, this estimate is the greatest source of error in the subsequent derivations. Two time dependent quantities, the FUV$-$B color and log (N_{Lyc}/L_{FUV}) , are derived for each region after correction for Galactic foreground extinction. The latter quantity is the logarithmic ratio of the number of Lyman continuum photons, converted from Hα flux assuming Case B recombination, to FUV flux. The observed FUV flux, FUV$-$B color, and log (N_{Lyc}/L_{FUV}) are listed in Table 5 along with the aperture sizes.

5.2. Derived Ages and Extinctions

The two time dependent parameters, FUV$-$B color and log (N_{Lyc}/L_{FUV}), are compared to model values allowing a simultaneous determination of the characteristic age and internal extinction of each region. This method is used to estimate the ages of H II regions in M81 (Hill *et al.* 1995) and NGC 4449 (Hill *et al.* 1998) where it is described in detail. A single generation instantaneous burst (IB) model, assuming the stellar evolutionary tracks of the Geneva group (Schaerer *et al.* 1993) and the stellar atmosphere models of Kurucz (1992), is used. The model estimates L_{FUV}, N_{Lyc}, and L_B for an evolving cluster

TABLE 5
DERIVED PROPERTIES OF STAR FORMING REGIONS

Region #	Aperture (″)	FUV Flux[a]	FUV−B	O5 V Stars[b]	Age Group	$E(B-V)_i$	A_{FUV}[c]
1	16.0	63.8	−3.18	24	1	0.07	0.63
2	16.0	41.4	−3.22	11	2	0.03	0.27
3	16.0	31.3	−3.45	7	2	0.0	0.0
4	25.6	168.2	−3.27	50	2	0.04	0.36
5	9.6	30.3	−3.34	10	1	0.05	0.45
6	22.4	122.9	−3.19	47	1	0.07	0.63
7	16.0	62.7	−2.97	28	1	0.09	0.81
8	28.8	67.5	−3.25	17	2	0.02	0.18
9	51.2	414.4	−3.15	172	1	0.08	0.72
10	19.2	19.9	−2.72	11	2	0.12	1.08
11	12.8	9.1	−3.04	2	3	0.02	0.18
12	22.4	37.3	−2.97	12	3	0.05	0.45
13	22.4	43.1	−2.53	18	4	0.08	0.72
14	22.4	67.9	−2.92	26	3	0.07	0.63
15	16.0	40.9	−3.09	9	3	0.01	0.09
16	16.0	22.0	−3.27	7	2	0.04	0.36
17	19.2	74.0	−3.04	22	2	0.04	0.36
18	19.2	67.8	−2.99	19	3	0.03	0.27
19	16.0	50.0	−3.08	11	3	0.0	0.0
20	16.0	33.4	−3.18	7	3	0.0	0.0
21	16.0	33.0	−2.82	8	4	0.01	0.09
22	16.0	18.9	−2.72	9	3	0.09	0.81
23	25.6	47.5	−3.27	11	2	0.01	0.09
24	15.6	10.1	−3.43	4	1	0.07	0.63
25	25.6	9.6	−2.28	10	2	0.19	1.71
26	35.2	25.6	−2.75	16	2	0.13	1.17
27	25.6	33.7	−3.18	7	2	0.0	0.0
28	32.0	61.2	−2.89	14	4	0.01	0.09
29	25.6	17.9	−2.73	8	3	0.09	0.81
30	54.4	174.6	−2.89	44	4	0.02	0.18
31	25.6	12.7	−2.55	8	3	0.13	1.17
32	19.2	4.6	−2.47	3	2	0.15	1.35
33	25.6	55.4	−3.04	29	1	0.11	0.99
34	22.4	22.2	−2.99	6	3	0.03	0.27
35	47.6	138.3	−2.60	49	4	0.06	0.54
36	32.0	69.6	−2.60	21	4	0.04	0.36
37	48.0	115.3	−2.92	25	4	0.0	0.0
38	32.0	8.7	−2.42	10	2	0.20	1.80
39	25.6	9.5	−2.62	10	1	0.19	1.71
40	25.6	16.2	−3.12	5	2	0.05	0.45
41	19.2	13.1	−3.33	3	2	0.0	0.0
42	19.2	6.6	−2.71	4	2	0.13	1.17
43	19.2	4.3	−3.16	2	1	0.06	0.54
44	16.0	2.5	−2.40	2	2	0.17	1.53
45	16.0	2.7	−3.13	1	1	0.09	0.81

[a]FUV flux in units of 10^{-16}erg (cm^2Å s) $^{-1}$, corrected for Galactic foreground extinction only.

[b]Equivalent number of O5 V stars at assumed galaxy distance, derived from internal extinction corrected FUV flux.

[c]Internal extinction derived via LMC redenning law.

over 100 Myr with a 0.5 Myr timestep. These parameters are then integrated over the each of the observed bandpasses. Several assumptions are made to simulate the environment in HoII. A mass range of 1 $-$ 100 $M_\odot$ for model stars is assumed. Under the assumption that regions are forming O-type stars, a relatively flat slope for the model IMF is chosen. A slope of -1.08, derived by Hill *et al.* (1994) for Lucke-Hodge regions in the vicinity of the 30 Dor region in the LMC, is used. However, the subsequent age derivations are not very sensitive to differences in the IMF. For example, using a model with a slope of -1.0 and one with -2.0 only results in small differences in the internal extinction estimates. At maximum, an underestimation of the extinction by E(B$-$V)=0.01 for stars 3.5 $-$ 10 Myr would result. However, differences in the assumed cluster metallicity show substantial differences in the shape of the model relationship. An LMC-like metallicity, $Z/Z_\odot = 0.4$, is assumed.

The observed values of FUV$-$B and log (N_{Lyc}/L_{FUV}) are corrected with an array of E(B$-$V)'s assuming a LMC curve, chosen under the assumption that the shape of the curve correlates with metallicity (Verter & Rickard 1998). In the FUV, $A_{FUV}/E(B-V)=9.04$ for the LMC extinction curve (Hill *et al.* 1997). The array of corrected observations for each region are compared to the model plot. Since the corrected data points are tied to E(B-V) values and the model is age dependent, the point at which a corrected value agrees with the model curve gives both an age and internal extinction estimate. To illustrate this method, the LMC model for t= 0 $-$ 50 Myr is shown in Figure 7 with several regions. The region number represents the uncorrected data point; the dashed line connecting it to the model represents the array of corrected values. The length of the dashed line is a measure of the internal extinction and the point at which it crosses the model is the approximate age of the cluster.

The age obtained using this method should be treated as the mean age of stars in the aperture due to the fact that a single generation model is used to interpret flux from what is potentially a mix of populations of slightly different ages. To compensate for this uncertainty, regions are classified into four age groups. These groups result from both the shape of the model and how the observations are naturally grouped with one another. This range is sufficient to establish the relative ages of regions for large scale comparisons and to identify star formation patterns. The age groups are shown in Figure 7 by the alternating dotted and solid lines of the model: group 1 (first dotted line) = 0 $-$ 3.5 Myr, group 2 (first solid line) = 3.5 $-$ 4.5 Myr, group 3 (next dotted line) = 4.5 $-$ 6.3 Myr; group 4 (last solid line) $\geq$ 6.3 Myr. When comparing regions, the actual age cutoffs for each group should be ignored and groups should be thought to consist of relatively very young, young, intermediate age, or older star forming regions for groups 1 $-$ 4, respectively. The derived age groups and internal extinctions are listed for each region in Table 5.

The ages of star formation regions are plotted on the FUV image to reveal the spatial distribution of star formation as a function of age in Figure 8. The ages are identified by a symbol, representing the mean age of stars within the circular aperture of like size. Two locations in the galaxy generally contain the youngest regions, the eastern side of the central arc and the linear group at the southern part of the galaxy. Using Figure 6 to reference the region numbers, these are region numbers 38 $-$ 45 and 1 $-$ 9, respectively. However, the young regions are not restricted to these two areas. The youngest derived age, $\sim$ 2.4 Myr, is located on the western side of the galaxy (region 24) adjacent to the oldest group of regions. Being a strong, compact Hα source and lacking FUV emission, the young age of this region is not surprising while its location seems somewhat peculiar. The older regions in the galaxy are mostly the larger, diffuse regions in areas of less concentrated star formation (regions 30, 35 $-$ 37). The oldest region, region 37, has a derived age of $\gtrsim$ 10 Myr. It is most likely much older than this, but difficulties in measuring the Hα flux at this level do not allow the limit to be constrained further. The origin of diffuse FUV emission found in a galaxy is sometimes hard to determine. Possible sources include scattering from dust grains and light from a spatially unresolved population of hot stars. In a low metallicity galaxy with low global extinction, scattering of UV light is not problematic and allows direct imaging of high-mass star formation. Therefore, the diffuse light in the larger apertures is most likely a spatially dispersed population of B stars formed over the past few 100 Myr.

The derived internal extinctions, A_{FUV}, in Table 5 show several trends when compared to their respective age groups. Age groups 1 $-$ 3 show a full range in extinction, $A_{FUV} \sim 0 - 2$ while regions in group 4 have substantially lower extinctions, generally $A_{FUV} \lesssim 0.3$. Extinction estimates for individual

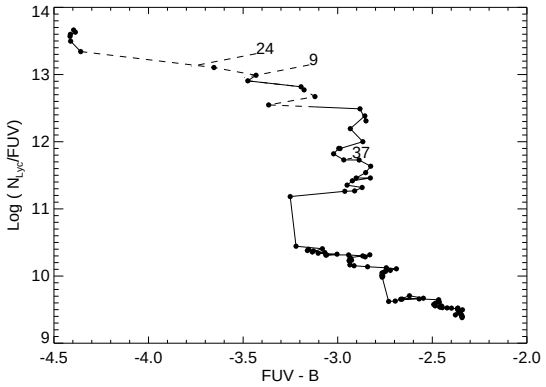

Fig. 7.— Cluster model with three Holmberg II data points. The uncorrected data points are represented by the region number. The age groups are shown by the alternating dotted and solid lines of the model: group 1 (first dotted line) = 0 − 3.5 Myr, group 2 (first solid line) = 3.5 − 4.5 Myr, group 3 (next dotted line) = 4.5 − 6.3 Myr; group 4 (last solid line) ≥ 6.3 Myr.

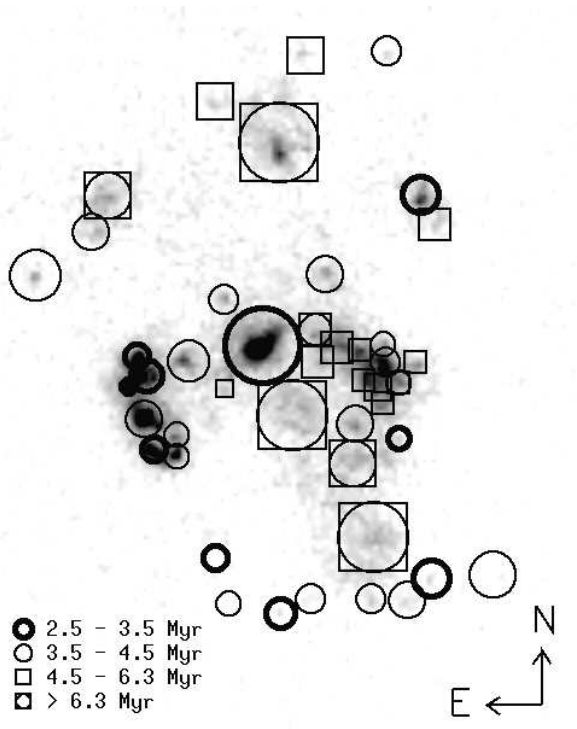

Fig. 8.— Derived ages of Holmberg II star forming regions plotted on the FUV image.

star forming regions derived from H_α/H_β line ratios for dwarf galaxies, including 4 regions in HoII, also fall in this range (Hunter & Gallagher 1985). Extinction proves to be quite patchy when comparing the spatial distribution of extinction levels. This distribution can be reconciled with the shell-like HI morphology of the galaxy (discussed in §7). The highest extinction levels are found in the dense HI ridges and the lowest levels in the HI voids. There is often not a smooth transition between extinction levels of adjacent regions. The distribution of internal extinction levels in HoII illustrates the problematic nature of using a global correction in irregular galaxies, especially those with HI shell structures.

5.3. Number of O Stars

To further quantify the FUV fluxes in individual star forming regions, the number of equivalent early-O type main sequence stars is derived from the internal extinction corrected FUV flux of each region and listed in Table 5. This exercise allows a comparison between the relative stellar content of regions to the first order. The derivation is based on the M_{FUV} for normal stars in the UIT bandpasses from the Fanelli *et al.* (1992) stellar library. To derive the equivalent number of stars per a given region, the expected flux of a single O5 V star is scaled to the galaxy's distance and compared to the corrected FUV flux. A single O5 V star is $M_{FUV}(B1)=-10.2$; its unextincted magnitude at the distance of HoII is $m_{FUV}(B1)=17.2$.

An equivalent number of 172 early-O type stars is estimated for the most energetic complex in HoII, region 9. This number is comparable to, but slightly less than, the number generally accepted to be present in the central $(1' \times 1')$ 30 Dor complex in the LMC, $\sim$ 230 (Vacca *et al.* 1995). Using FUV data, Hill *et al.* (1997) estimate that the brightest regions in Sbc spiral M51, Rand 308 and 78, have an equivalent number of 245 and 242 early-O type stars, respectively. Holmberg II is dominated by one large complex which is able to produce a prodigious amount of star formation comparable to that in much larger galaxies. Even the large, FUV diffuse regions have a significant equivalent number of early-O type stars present. For example, the diffuse FUV flux in region 35 is equivalent to 49 O5 V stars.

6. Massive Stars and the Local ISM

Massive stars dump energy into their surrounding ISM via ionizing photons, supernovae explosions, stellar winds, and outflows. Combined, these processes have a profound affect on the surrounding region of gas. The ionizing photon bath alone, provided by UV photons from massive stars, can deposit prodigious amounts of kinetic energy into the ISM. The "champagne" model (Tenorio-Tagle 1979), summarized by Hunter (1992), describes the process by which massive stars ionize their surrounding gas creating compact HII regions that evolve into extended objects. As the ionization front reaches the edge of the parental molecular cloud, ionization of the neutral medium commences, where by the stars lie in a half-open cavity in the dense cloud and the HII region emerges as a "blister" on the side of the cloud. Numerous observationally-based studies support both the existence of champagne flows and the premise that expanding ionized structures are caused by localized energy sources (Lafon *et al.* 1983; Heydari-Malayeri & Testor 1981). A tedious approach to identifying massive stars inside ionized structures can be made through spectroscopy. Optical observations of massive stellar populations, the less massive remnants of the population actually responsible for the expanding features, have been employed to compare the energy available from the population with the ionization and formation requirements of the expanding ionized structures (Hunter *et al.* 1995). In contrast, Parker *et al.* (1998) use UIT observations of the LMC and SMC to identify the hottest OB stellar members, those responsible for the majority of the ionizing flux, and correlate the FUV photometry of these stars with the Hα flux of the associated HII regions.

6.1. Morphology of Massive Stars and Ionized Gas

Several examples illustrating the relationship between massive stars and ionized structures in various evolutionary stages are found in HoII. Figure 9 shows registered Hα and FUV images of region 6. The shell in the center of the Hα image encircles a group of massive stars present in the FUV image providing evidence of a causal relationship. The emission on the edges of the Hα shell itself is not symmetrical; the emission on the left side of the shell is more prominent than on the right, consistent with the champagne model. Region 9 presents similar evidence in Figure 10 where a more complex system of shells is present, suggesting that a less spatially concentrated group of massive stars is responsible for the ionization. The FUV image identifies the distribution of these stars, a $\sim$ 400 pc chain decreasing in intensity from the lower right to the upper left. The FUV luminosity of this region indicates the presence of an equivalent number of 172 O5 V stars; an average age of $\sim$ 3.3 Myr is estimated for the entire complex.

6.2. Local Triggering Mechanisms

As illustrated by Elmegreen & Lada (1977), the high pressures generated by stellar winds, ionized gas, and supernovae explosions can act as a triggering mechanism to convert stable configurations of gas to unstable ones. The ionization front emerging from a star formation complex is followed by a shock front generated by the supersonic flow of the ionized material. If formed on the edge of a molecular cloud, the successive passage of ionization and shock fronts into a neighboring cloud allows unstable configurations of dense neutral material to accumulate to form new stars. These stars generate new ionization fronts and the cycle continues (Blaauw 1991). Massive star formation has the ability to influence the formation of new sites of star formation creating linear sequences of stellar subgroups within OB associations, potentially allowing self-propagation throughout a region.

The cumulative chain reactions initiated by these local events have been suggested as an overall mechanism for star formation in irregular galaxies. First proposed by Gerola & Seiden (1978) as a global mechanism for star formation, the stochastic self-propagating star formation model (SSPSF) describes the propagation of star formation between neighboring regions by means of a "percolation" process. Gerola *et al.* (1980) adapt the SSPSF to small galaxies with no differential rotation and find the model predicts characteristics which correlate nicely with those of dwarf galaxies. In particular, the model produces galaxies that form stars in a bursting mode of short-lived episodes and a SFR that varies drastically with time. While the average SFR's are low, the galaxies have instantaneous SFR's that range from bursting to quiescent, which could explain the diverse star formation characteristics observed in dwarf galaxies. However, a recent survey of 110 Virgo dwarf irregulars indicates that star formation is generally preferential to the edges, mostly to one side of the galaxy, while the SSPSF model does not predict pat-

terns that predominately favor any particular location (Brosch, Heller, & Almoznino 1998).

Sequential star formation has been documented observationally in galaxies of similar type as the present sample (Lortet & Testor 1988; Dopita *et al.* 1985). On local scales (within the same molecular cloud), sequential star formation can be inferred by observations of two spatially adjacent regions with slight age differences. Comparisons of Hα and FUV emission morphologies can indicate the relative ages of adjacent young star formation sites due to the longer timescale of decay of the FUV emission in a given region. The relationship between the Hα and FUV flux as a function of time for a given cluster is shown in Figure 11 illustrating the physical basis for this qualitative treatment of relative cluster ages. A relatively strong FUV source surrounded by compact HII regions is suggestive of sequential star formation using this method. Region 23, shown in Figure 12, exemplifies this scenario. The region, having an average age of $\sim$ 4.3 Myr, consists of two compact HII regions surrounding a relatively strong FUV source. The group of regions on the western side of the central star forming arc (regions 15-22), shown in Figure 13, illustrates the geometry of sequential star formation as suggested by the SSPSF model. Age estimates of the individual regions show a mix of age groups 2$-$4. A chain of young star formation seen on the Hα image is located to the right of a faint chain of FUV emission suggesting star formation is propagating from left to right.

7. Large-Scale Triggering Mechanisms

Massive star formation can influence new star formation activity on larger scales as high pressures from supernovae push gas away from aging OB associations. In theory, when a star forming complex has sufficient numbers of main sequence O and B stars, the combined pressures from stellar winds and supernovae are able to drive an expanding ionized shell of gas and at the same time, create a void in the neutral gas (Tenorio-Tagle & Bodenheimer 1988). Sequential star formation typically acts on only one side of a molecular cloud where as large-scale triggering describes the process by which a centralized source destroys the remainder of its parental molecular cloud, creating a void in the gas and a dense ridge of swept up material carried to large distances (Weaver *et al.* 1977). Described by Elmegreen (1992)

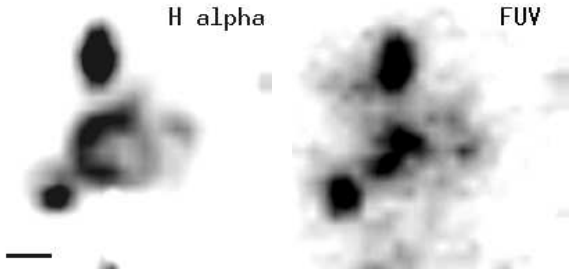

Fig. 9.— Registered Hα and FUV images of Holmberg II, region 6. The dark bar in the lower left-hand corner represents 100 pc in Figures 9, 10, 12, and 13.

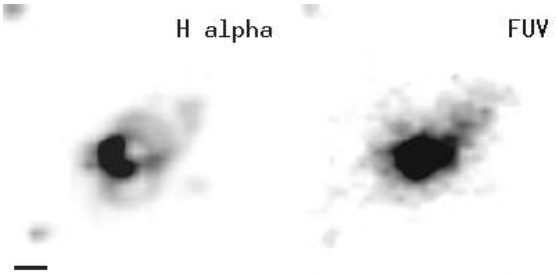

Fig. 10.— Registered Hα and FUV images of Holmberg II, region 9.

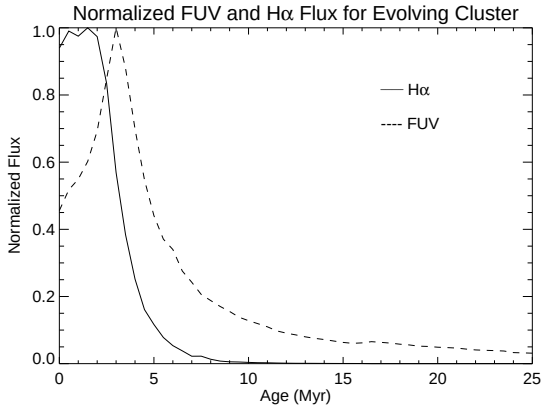

Fig. 11.— Normalized FUV and Hα flux for an evolving star cluster.

as the "collect and collapse" method, dynamical instability of the accumulated gas collapses under self gravity to form new stars along the periphery of the shell. This scenario is a plausible explanation for the correlation between stellar age and proximity to the HI shell boundary in dwarf galaxy Sextans A, where the youngest stars are primarily found in the interior of the HI shell (Van Dyk, Puche, & Wong 1998). The ridge surrounding a swept-up shell may fragment leaving chains or arcs of new star formation, allowing a means for star formation to propagate on large scales. Efremov & Elmegreen (1998) recently demonstrated that two arcs of clusters inside and on the rim of the superbubble LMC4 in the LMC, which surrounds a roughly 30 Myr-old dispersed group of supergiants and Cepheid variables, may have been formed by the self-gravitational collapse of gas in swept-up pieces of rings or shells. On smaller scales, feedback from massive star formation is also evident in HI data, such as the turbulent and fractal nature of the local ISM shown by the HI mosaic of the LMC (Kim *et al.* 1998).

Puche *et al.* (1992) point out that the observed radial expansions, energy requirements and kinematic ages of the holes in HoII indicate that they originate from internal, pressure driven events. Radio continuum observations of HoII confirm that supernovae do lie within several HII regions (Tongue & Westpfahl 1995). Further analysis indicates that the supernovae energy injection rate into the galaxy is sufficient to account for the global number of HI features. On the other hand, numerical simulations using hydrodynamic methods to simulate powerful local energy sources have failed to reproduce all the features in the neutral medium of HoII (Maschenko & Silich 1995). Some of the HI holes in HoII, especially those located beyond the optical disk of the galaxy, are likely formed by alternate mechanisms such as gravitational instability via collisional dissipation of gas particles (Byrd & Howard 1992) or infall of gas clouds (van der Hulst & Sancisi 1988). Rhode *et al.* (1999) identify a single high velocity cloud candidate in their HI data. However, the distribution of holes is too regular and present at all radii to be explained entirely by infall. Other environmental factors, such as tidal perturbations, are not a factor due to the fact that HoII is fairly isolated.

The closest neighbor to HoII is M81 dwarfA (Kar 52). Given that the kinematic HI mass of HoII is a factor of 100 greater than that of M81 dwarfA (Melisse & Israel 1994), it is unlikely to have affected HoII. Moreover, M81 dwarfA is at a distance on the sky of roughly 27 kpc from HoII with a relative radial velocity of 44 km/s. The current tidal perturbation of HoII due to this neighbor will be very tiny compared to the internal gravitation. Using the values of the known components of position and velocity along with the masses, a positive two body orbital energy is obtained. The calculated value is less than the actual positive value if the unknown components of position and velocity were included. Thus, analysis of the orbital energy indicates that the companion is likely to be in a hyperbolic orbit. There is not a high probability of a close encounter, especially a prolonged one. The hyperbolic relative velocity with HoII indicates that an interaction might have happened $\sim$600 Myr ago, roughly three rotation periods within 1.8 kpc (the majority of the optical portion of the galaxy). This timescale is sufficient for the effects of a weak interaction to have dissipated via differential rotation.

Rhode *et al.* (1999) search for the lower-mass remnants of the population which in theory created the HI holes in several dwarf galaxies, including HoII. They estimate the expected number of A and F main sequence stars from the kinematic ages of the holes and the energy required for their creation. They do not find sufficient numbers of these stars in the HI holes in deep optical searches to support the stellar wind/supernovae scenario, although the expected number is dependant upon the choice of IMF. In addition, Massey *et al.* (1996) find that the UV-bright stars in M33 are evolved B supergiants indicating that the optically brightest stars are not necessarily the ionizing sources. Since FUV observations isolate the massive stellar component on timescales similar to the kinematical ages of HI holes, they can provide an observational "smoking gun" to the theoretical concept of pressure driven shells. Instead of searching for a requisite number of lower-mass neighbors, a search for the progenitor stars themselves can be made. In addition, FUV observations can show sites of secondary star formation in the dense ridges, allowing insight into the possibility that star formation triggering via giant HI shells is a viable mechanism for star formation. FUV observations have the potential to provide a snapshot of a full cycle of propagating star formation.

7.1. Relative FUV and HI Morphology

The numerous voids in the HI morphology of HoII are evident on the 21cm map presented in Figure 14; the FUV surface brightness contours are overplotted on the image. The large spatial extent of the HI disk is also apparent, extending well beyond both the FUV and optical disks. The HI holes are distributed evenly across the entire HI distribution including regions extending beyond the stellar disk. The largest hole is a ~ 1.7 kpc diameter void with a dense ridge in the southern part of the galaxy.

Since the expansion velocities of the HI holes were likely greater in the past, estimates of the kinematic ages using present day expansion rates yield upper limits. Puche *et al.* (1992) derive ages for the HI holes ranging from $26 - 136$ Myr assuming a constant expansion rate. Given these ages, some measure of FUV emission should be spatially coincident with the voids if they are caused by massive star formation. Even if only the most massive stars are responsible for the generation of the HI holes, their less massive neighbors (early B-type stars) would still be detectable on the FUV images. However, the existence of HI holes beyond the stellar disk is not consistent with the supernovae/stellar wind scenario for their creation unless a very unusual IMF is present in the outer parts of the galaxy. It is likely that an alternate mechanism is responsible. However, this mechanism is not a viable feedback mechanism for new star formation due to the absence of dense rims and corresponding secondary sites on the periphery of these holes.

The lack of FUV emission in the centers of HI holes in the outer parts of HoII does not disprove the generation of large shells by massive stars since several HI voids in the inner part of the gas distribution are coincident with FUV emission. In addition, density enhancements along the rims of HI shells correspond to sites of FUV emission suggestive of propagating star formation. The largest HI hole illustrates the connection between two generations of star formation. The FUV-bright central star forming arc is aligned with the northern rim of this HI hole, while diffuse patches of FUV emission lie within its boundary. Other examples of FUV emission coincident with HI voids are the eastern two patches in the northern part of the galaxy. Several of the second generation sites also show they are beginning to disrupt the surrounding gas. For example, the intense star formation on the eastern edge of the central arc has HI density enhance-

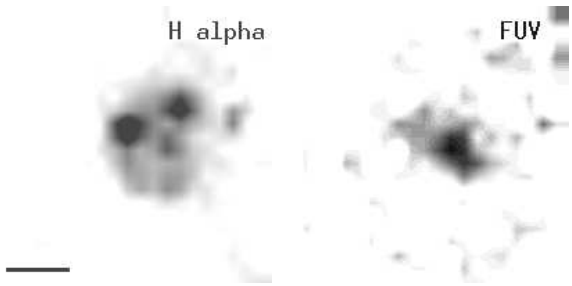

Fig. 12.— Registered Hα and FUV images of Holmberg II, region 23.

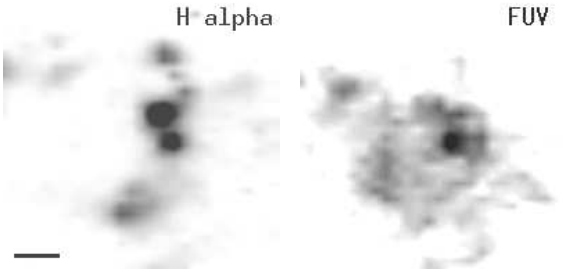

Fig. 13.— Registered Hα and FUV images of Holmberg II, regions 15-22.

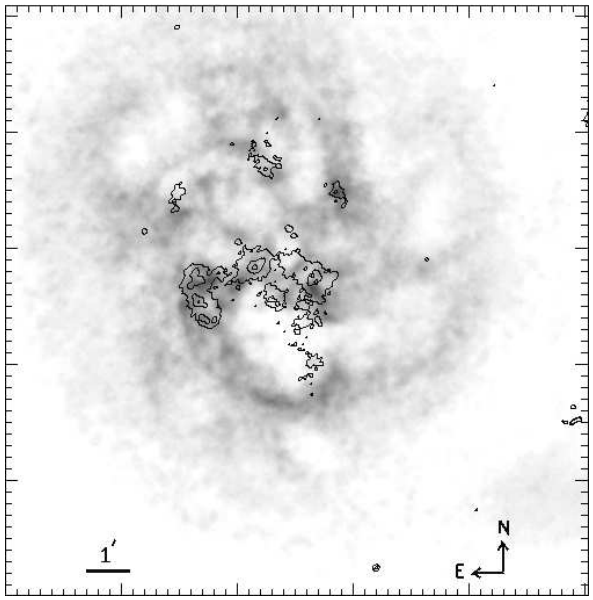

Fig. 14.— HI image of Holmberg II overplotted with the 19, 20, and 21.8 mag arcsec^{-2} FUV surface brightness contours.

ments located on either side. Tongue & Westpfahl (1995) confirm the existence of supernovae inside star forming regions in this area (regions 1, 4, and 6) using radio continuum observations. These supernovae are likely responsible in part for reshaping the surrounding neutral medium. Photodisassociation of H_2 on the interior of surfaces of the molecular cloud may also be responsible for the HI density enhancements surrounding the intense young star forming regions to a certain degree. However, Tacconi & Young (1987) do not detect any ^{12}CO emission above the 3σ level in HoII. Lacking other observations to trace the molecular component, its morphology remains a mystery. In general, evolved star forming knots are fairly efficient in converting in converting H_2 to HI (Allen *et al.* 1987).

The derived ages for individual star forming regions further illustrate the connection between massive star formation and the HI morphology. The age groups for individual star formation regions are displayed in Figure 15 on the HI map. Each of the seven regions in the oldest age group (group 4, > 6.3 Myr), lies in a HI hole or local minimum in the HI density. The largest hole contains three large regions in age group 4 on the western side of its interior. The youngest regions (group 1, $2.5 - 3.5$ Myr) are each spatially coincident with HI density enhancements suggesting the potential for new star formation is high on the dense rims of the HI holes. The majority of new star formation in the whole system is occurring on the periphery of the largest hole. The distribution of star formation ages in general can be interpreted by this comparison. The spatial proximity of a very old region and a very young one is reconciled by the HI density distribution.

7.2. HI Hole Energetics

A quantitative approach to test the observational evidence suggesting that massive star formation triggers holes in the neutral medium is offered by comparing the energy delivered to the ISM by massive stars and the required creation energy of the HI holes. FUV observations of the clusters interior to the HI holes provide an estimate of the total mechanical energy delivered to the ISM, assuming the derived ages and internal extinctions. Several of these clusters are spatially coincident with HI holes included in the Puche *et al.* (1992) study where estimates for their creation energy, E_o, are given. These hole/cluster combinations are listed in Table 6. Region numbers refer to

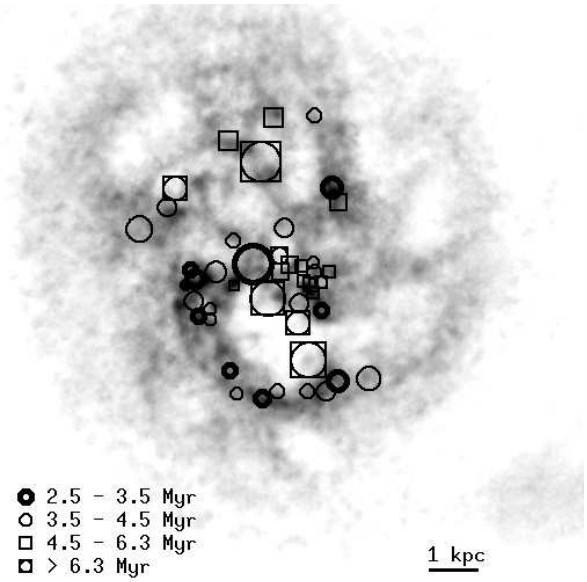

Fig. 15.— HI image of Holmberg II shown with the derived ages of star forming regions.

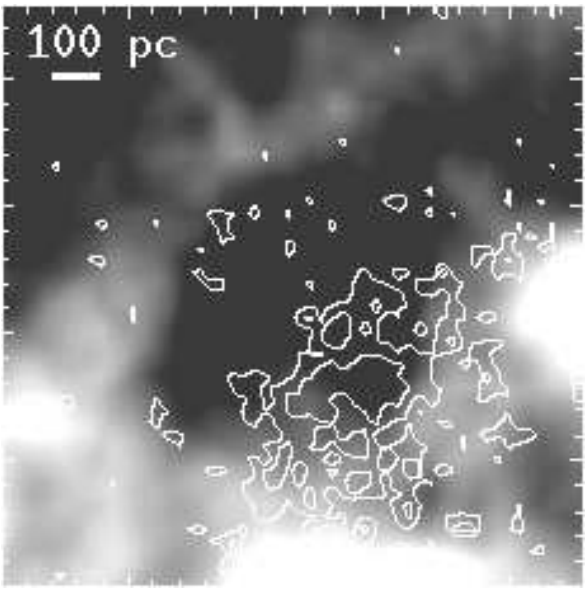

Fig. 16.— HI image of Holmberg II region 28 overplotted with the 21.5 and 22 mag arcsec^{-2} FUV surface brightness contours. Figures 16−18 are displayed so that the HI holes appear as dark voids and the HI density enhancements are bright.

the previously defined star formation regions and hole numbers are taken from Puche *et al.* (1992). For reference, HI images showing each hole used in this comparison are presented with the FUV contours in Figures 16-18.

The observed FUV luminosity, L_{FUV}, for each cluster is estimated from the FUV flux and internal extinction correction given in Table 5. Cluster mass is estimated by comparing the observed L_{FUV} with the model of L_{FUV} (ergs s^{-1} $M_{\odot}{}^{-1}$) for an evolving cluster at the given cluster age. This model is used to derive the ages and internal extinctions for all star formation regions and described previously (§5.2). The mechanical energy deposited into the ISM, L_{mech}, over a timescale equal to the age of the cluster can be calculated assuming a rate which is a function of cluster mass. Evolutionary synthesis models of populations of massive stars given by Leitherer & Heckman (1995) provide estimates of the deposition rates from stellar winds and supernovae for an instantaneous burst as a function of time and mass. From clusters of similar IMF and metallicity, an average rate of $L_{mech} \sim 3 \times 10^{34}$ ergs (s $M_{\odot})^{-1}$ is assumed. The net mechanical energy deposited into the ISM by supernovae and stellar winds, E_{SN}, is estimated assuming this rate, the total cluster mass, and the derived cluster age.

The derived properties of the clusters spatially coincident to HI holes are given in Table 6. In each case, $E_{SN} > E_o$ indicating that to the first order, the energy provided by massive stars is sufficient to create the HI holes that encircle them. The largest hole (# 21) actually contains two star forming regions which are added together to estimate the energy input. All the star forming regions interior to HI holes are in the oldest age group (group 4, > 6.3 Myr). The derived ages in Table 5 for these regions are upper limits in the sense that these regions are likely much older. (The technique to derive the ages depends upon the presence of Hα emission and is not reliable for absolute ages >6.3 Myr.) For these regions, E_{SN} is a lower limit and would increase linearly with the true cluster age. Region 13 has significantly more energy than the creation energy of its associated HI hole. It is possible that this region is also responsible for an adjacent hole (# 22), which would increase E_o by 35×10^{50} ergs. These comparisons suggest that massive stars do provide sufficient mechanical energy to account for the observed properties of associated HI holes in HoII.

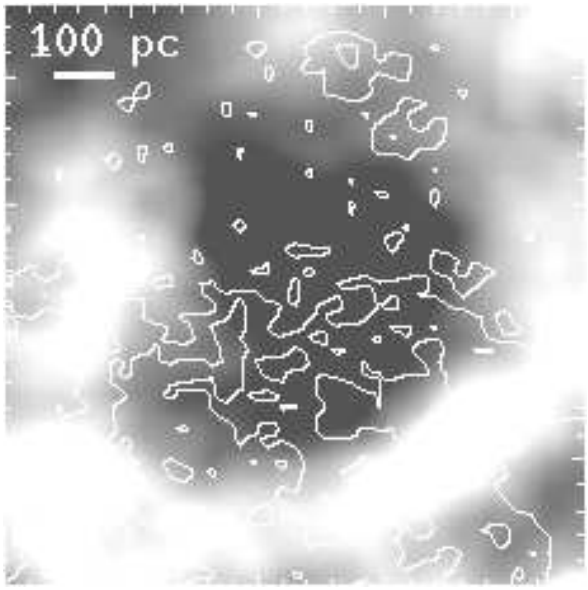

Fig. 17.— HI image of Holmberg II region 13 overplotted with the 21 and 21.7 mag arcsec^{-2} FUV surface brightness contours.

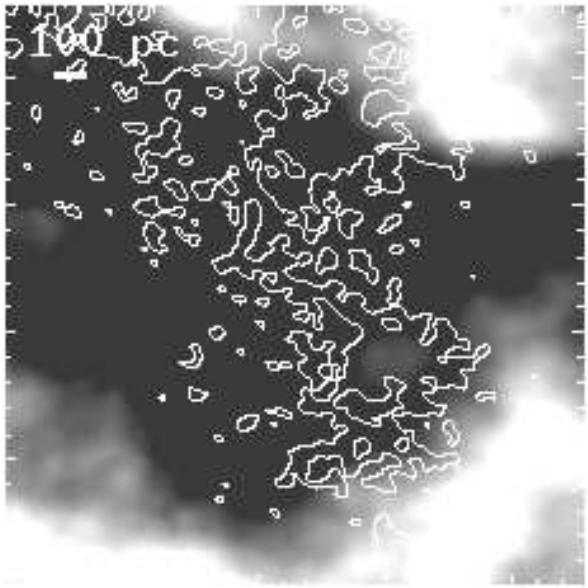

Fig. 18.— HI image of Holmberg II regions 36 and 37 overplotted with the 19, 20.5, and 21.75 mag arcsec^{-2} FUV surface brightness contours.

Reg #	Hole #	Age Myr	L_{FUV} 10^{36} ergs s^{-1}	Mass $10^3 M_\odot$	E_o 10^{50}ergs	E_{SN} 10^{50}ergs
28	48	8.5	7.4	7.57	470.3	608.8
13	23	8.5	9.3	9.53	41.1	766.4
36,37	21	10.0	23.6	32.10	2025	3036.9

Table 6: Derived Properties of Clusters in HI holes

NOTE.—Region numbers refer to clusters defined in Table 5. Data for the HI holes encircling a given cluster are taken from Puche *et al.* (1992) including hole numbers and creation energy, E_o.

7.3. Characteristic Differences in the ISM

The question remains: if massive star formation can provide sufficient energy to generate holes in the surrounding neutral medium, why are there not HI holes around every OB association? The answer may be related to global properties of the ISM. Characteristic differences in the kinematical properties of the ISM can be traced to differences in the star formation mechanisms.

Solid body rotation of the gas disk is a general property of dwarf galaxies which makes them appealing for star formation studies. The lack of shear in the absence of differential rotation allows features in the HI gas to be longer-lived. The thicker gas disks and lack of shear in irregulars allow the growth of larger gas clouds (Hunter 1997). This combination provides an excellent environment for stars to form in giant complexes. Since larger complexes impact the surrounding ISM to a greater degree and HI features survive longer in regions of reduced shear, HI holes and associated sites of secondary star formation are more likely to be found in areas of the gas disk exhibiting solid body rotation.

The rotation curve of HoII, taken from Puche *et al.* (1992) and displayed in Figure 19, exhibits solid body rotation to a radius of r$\sim 2'$ after which it flattens and exhibits differential rotation. An ellipse with a major axis of $2'$, reduced to the plane of HoII, is plotted on the FUV image of the galaxy in Figure 20. The majority of the FUV emission is contained within the ellipse. This is also the region where examples of large-scale star formation triggering via HI shells are found. This simple illustration demonstrates that massive star formation in HoII can operate more easily as a feedback mechanism in regions with uncomplicated global kinematical properties.

8. Summary

This study uses FUV, HI, and Hα observations of dwarf irregular galaxy HoII to trace the interaction between sites of massive star formation and the neutral and ionized components of the surrounding ISM and to identify the means by which star formation propagates in this intrinsically simple system. Both local and large-scale triggering mechanisms related to massive stars are identified suggesting that feedback from massive stars is a microscopic process operating in all galaxies to a certain degree.

The key results from the study can be summarized as follows:

(1) In comparison to its optical images, the FUV morphology of HoII is patchy and irregular. Massive star formation does not have a smooth spatial distribution; it is concentrated in several dominate complexes. The fact that massive star formation is not centrally organized has important implications for interpreting images of high redshift galaxies (z $\gtrsim$ 3) where the restframe FUV is detected using optical and IR instruments.

(2) Surface brightness profiles are used to characterize the radial dependence of the azimuthally averaged star formation activity. The FUV profile is generally flat with inflections due to prominent complexes. The B-band profile displays an exponential shape with a central light depression, characteristic of dwarf galaxies. The derived central surface brightness, $\mu_B(0)$, lies in the expected range for dwarf galaxies. Comparisons of profiles in the R, B, U and FUV bands indicate that profiles retain the same general shape while inflections due to star formation increase as the wavelength of the profile decreases. The radial continuity of star formation sites demonstrates that

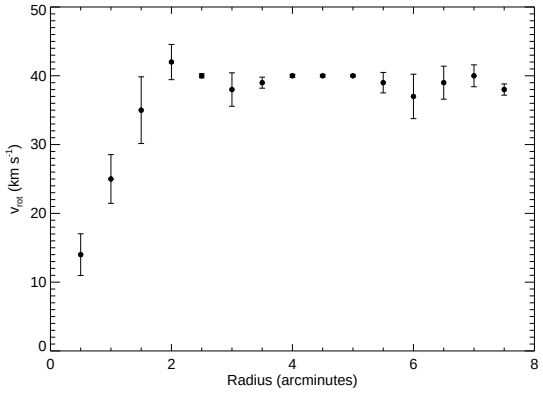

Fig. 19.— Holmberg II rotation curve taken from Puche *et al.* (1992).

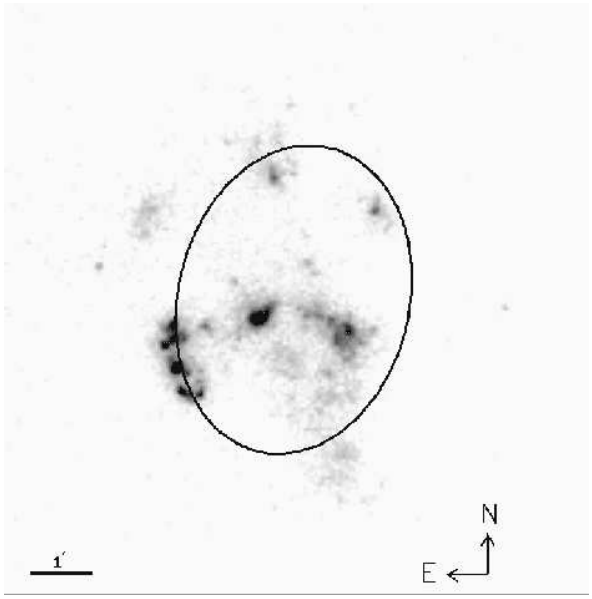

Fig. 20.— HI image of Holmberg II shown with a 2′ ellipse. The interior of the ellipse represents the solid body regime of the neutral gas disk.

the time averaged level of activity in the past correlates with the current activity at the same radius, supporting the theory that star formation in irregular galaxies is dominated by local processes.

(3) Star formation rates derived from Hα and FUV photometry are used to characterize the current (traced by Hα) and recent (traced by FUV) global star formation activity. Comparisons of the two rates allow a rough estimate of the recent star formation history and indicate that the galaxy is sustaining a somewhat recent star formation event.

(4) Ages for individual regions are derived using B, Hα, and FUV photometry and show both older, diffuse FUV regions and younger, compact HII regions. The distribution of ages is reconciled with the HI morphology, showing a clear preference of young regions for areas of dense HI and older regions for HI voids.

(5) Local star formation triggering mechanisms are identified via the relative Hα and FUV morphologies. Observational evidence of the influence that massive stars have on their surroundings includes massive stars inside ionized shells and compact HII regions surrounding aging clusters. Causal relationships between massive star formation and secondary sites of star formation are shown. Star formation progression patterns are consistent with the SSPSF model in that progressively older chains of star formation are seen in clusters.

(6) Large-scale star formation triggering by HI shells generated by massive stars is seen by comparing the FUV and HI morphologies. Given the timescale over which FUV observations trace massive star formation, both secondary sites of star formation and progenitor populations are identified. Analysis of the energy available from massive stars inside HI voids indicates that energy deposited into the ISM from supernovae and stellar winds are sufficient to account for the observed properties of the HI holes.

(7) Global kinematical properties may also play a role in the star formation process since differences in the rotation characteristics of the neutral gas disk are coupled with differences in triggering mechanisms. Large-scale feedback from massive star formation is shown to operate in regions that lack differential shear in the gas disk.

S.G.S. wishes to acknowledge the funding of this study through the Alabama Space Grant Consortium project and to thank the University of Alabama,

NASA/Goddard Space Flight Center, and the U. S. Naval Observatory for their support. Funding for the UIT project has been through the Spacelab Office at NASA Headquarters under project number 440-51.

REFERENCES

Allen, R. J., Knapen, J. H., Bohlin, R., & Stecher, T. P. 1997, ApJ, 487, 171

Blaauw, A. 1991, in *The Physics of Star Formation and Early Stellar Evolution*, ed. C. J. Lada & N. D. Kylafis, (Dordrecht: Kluwer), 125

Brosch, N., Heller, H., & Almoznino, E. 1998, MNRAS, 300, 1091

Byrd, G. G. & Howard, S. 1992, AJ, 103, 1089

Corwin, H. 1997, private communication

de Vaucouleurs, G., de Vaucouleurs, A., Corwin, H. G., Buta, R. J., Paturel, G., & Fouqué, P. 1991, Third Reference Catalog of Bright Galaxies (RC3) (New York: Springer)

Deharveng, J. -M., Sasseen, T. P., Buat, V., Bowyer, S., Lampton, M., & Wu, X. 1994, A&A, 289, 715

Dopita, M. A., Mathewson, D. S., & Ford, V. L. 1985, ApJ, 297, 599

Dressel, L. L. & Condon, J. J. 1976, ApJS, 31, 187

Efremov, Y. N. & Elmegreen, B. G. 1998, MNRAS, 299, 643

Elmegreen, B. G. 1992, in *Star Formation in Stellar Systems*, ed. G. Tenorio-Tagle & F. Sánchez (Cambridge: Cambridge University Press), 383

Elmegreen, B. G. & Lada, C. J. 1977, ApJ, 214, 725

Fanelli, M. N., *et al.* 1997a, BAAS, 191, # 82.01

Fanelli, M. N., O'Connell, R. W., Burstein, D., & Chi-Chao, W. 1992, ApJS, 82, 197

Fanelli, M. N., *et al.* 1997b, in *Star Formation Near and Far*, ed. S. S. Holt & L. G. Mundy (AIP Press), 598

Freeman, K. C. 1970, ApJ, 160, 811

Freedman, W. L., *et al.* 1994, ApJ, 427, 628

Gerola, H. & Seiden, P. E. 1978, ApJ, 223, 129

Gerola, H., Seiden, P. E., & Schulman, L. S. 1980, ApJ, 242, 517

Gessner, S. E., *et al.* 1995, BAAS, 187,# 11.06

Heydari-Malayeri, M. & Testor, G. 1981, A&A, 96, 219

Hill, J. K., *et al.* 1995, ApJ, 438, 181

Hill, J. K., *et al.* 1993, ApJ, 402, L45

Hill, J. K., Isensee, J. E., Cornett, R. H., Bohlin, R. C., O'Connell, R. W., Roberts, M. S., Smith, A. M., & Stecher, T. P. 1994, ApJ, 425, 122

Hill, J. K., *et al.* 1997, ApJ, 477, 673

Hill, R. S., *et al.* 1998, ApJ, 507, 179

Hodge, P., Strobel, N., & Kennicutt, R. C. 1994, PASP, 106, 309

Hoessel, J. G., Saha, A., & Danielson, G. E. 1998, AJ, 115, 573

Huchtmeier, W. K., & Richter, O.-G. 1988, A&A, 203, 237

Hunter, D. A. 1992, in *Star Formation in Stellar Systems*, ed. G. Tenorio-Tagle & F. Sánchez (Cambridge: Cambridge University Press), 66

Hunter, D. A. 1997, PASP, 109, 937

Hunter, D. A., Boyd, D. M., & Hawley, W. N. 1995, ApJS, 99, 551

Hunter, D. A., Elmegreen, B. G., & Baker, A. L. 1998, ApJ, 493, 595

Hunter, D. A. & Gallagher, J. S. 1985, ApJS, 58, 533

Hunter, D. A., Gallagher, J. S., Rice, W. L., & Gillett, F. C. 1989, ApJ, 336, 152

Karachentseva, V. E., Prugniel, P., Vennik, J., Richter, G. M., Thaun, T. X., & Martin, J. M. 1996, A&AS, 117, 343

Kennicutt, R. C. 1998, ARA&A, 36

Kim, S., *et al.* 1998, ApJ, 503, 674

Kurucz, R. L. 1992, in *Stellar Populations of Galaxies*, eds. B. Barbuy & A. Renzini, (Dordrecht:Kluwer), 225

Lafon, G., Deharveng, L., Baudry, A., & de La Nöe, J. 1983, A&A, 124, 1

Leitherer, C. & Heckman, T. M. 1995, ApJS, 96, 9

Lortet, M.-C. & Testor, G. 1988, A&A, 194, 11

Madau, P., Pozzetti, L., & Dickinson, M. 1998, ApJ, 498, 106

Maschenko, S. Y. & Silich, S. A. 1995, Astronomy Reports, 39, 587

Massey, P., Bianchi, L., Hutchings, J. B., & Stecher, T. P. 1996, ApJ, 469, 629

Melisse, J. P. M. & Israel, F. P. 1994, A&A, 285, 51

Miller, B. W. & Hodge, P. 1994, ApJ, 427, 656

Nilson, P. 1973, Uppsala General Catalogue of Galaxies (Uppsala Astr. Obs. Ann., 6)

O'Connell, R. W. 1997, in *The Ultraviolet Universe at Low and High Redshift*, ed. W. H. Waller, Fanelli, M. N., Hollis, J. E., & Danks, A. C., (AIP Press), 11

Page, T. & Carruthers, G. R. 1981, ApJ, 248, 906

Parker, J. Wm. 1998, AJ, 116, 180

Patterson, R. J. & Thuan, T. X. 1996, A&AS, 107, 103

Puche, D., Westpfahl, D., Brinks, E., & Roy, J.-R. 1992, AJ, 103, 1841

Rhode, K. L., Salzer, J. J., Westpfahl, D. J., & Radice, L. A. 1999, AJ, 118, 323

Rönnback, J. and Bergvall, N. 1994, A&AS, 108, 193

Ryder, S. D. & Dopita, M. A. 1994, ApJ, 430, 142

Salpeter, E. E. 1955, ApJ, 121, 161

Savage, B. D. & Mathis, J. S. ARA&A, 17, 73

Schaerer, D., Meynet, G., Maeder, A., Schaller, G. 1993, A&AS, 98, 523

Stecher, T. P., *et al.* 1992, ApJ, 395, L1

Stecher, T. P., *et al.* 1997, PASP, 109, 735

Stewart, S. G. 1998, Ph.D. Thesis, University of Alabama

Stone, R. P. S. 1977, ApJ, 218, 767

Tacconi, L. J. & Young, J. S. 1987, ApJ, 322, 681

Tenorio-Tagle, G. 1979, A&A, 71, 59

Tenorio-Tagle, G. & Bodenheimer, P. 1988, ARA&A, 26, 145

Tongue, T. D. & Westpfahl, D. J. 1995, AJ, 109, 2462

Vacca, W. D., Robert, C., Leitherer, C., & Conti, P. S. 1995, ApJ, 444, 647

Vader, J. P. & Chaboyer, B. 1994, AJ, 108, 1209

van den Bergh, S. 1959, Publ. David Dunlap Obs. II, No. 5

van der Hulst, T. & Sancisi, R. 1988, AJ, 95, 1354

Van Dyk, S. D., Puche, D., & Wong, T. 1998, AJ, 116, 2341

Verter, F. & Rickard, L. J. 1998, AJ, 115, 745

Waller, W. 1990, PASP, 102, 1217

Weaver, R., McCray, R., Castor, J., Shapiro, P., & Moore, R. 1977, ApJ, 218, 377

Westpfahl, D. 1997, Private Communication

This 2-column preprint was prepared with the AAS LaTeX macros v4.0.